Chapter 3
Titanium-Based Mesoporous Materials for Photocatalysis

3.1 The History of Mesoporous Materials

Up to date, it is well known that the rapid progress of society is closely associated with material science. Particularly in recent 30 or 40 years, there has been a boom of novel materials, including of mesoporous materials. Mesoporous molecular sieve belongs to a noticeable area owing to its excellent properties, such as high specific surface area and adjustable ordered mesoporous pore size. According to the rules of IUPAC, porous materials can be classified into three types: micropore materials (pore size <2 nm), mesopore materials (2 nm <pore size <50 nm), and macropore materials (pore size >50 nm), respectively [1]. In 1992, the Mobil's researchers successfully synthesized a novel ordered mesoporous silica materials called M41S with surfactants as templating agents, thus opening a new era of mesoporous materials [2]. On the basis of chemical composition, mesoporous molecular sieve can be divided into two categories: silicon-based materials and non-silicon-based materials. The most common one is M41S, which is a branch of silicon-based materials. Additionally, there are many other sorts of mesoporous molecular sieves, such as SBA-n series, MSU series, CMK series, HMS, KIT, and metallic or metal oxide series. Compared with microporous and macroporous molecular sieves, mesoporous materials possess many outstanding characteristics. But there are still some shortcomings exist, for instance, its low hydrothermal stability and weak acidity, which limit its application. Ryoo et al. [3] synthesized highly stable MCM-41 by adjusting the pH value of the solution and adding salt compounds. And Mokaya et al. [4] obtained ultrastable MCM-41 by post-processing. Robert Mokaya prepared restructured pure silica MCM-41 materials through seeded crystallization route. This method used MCM-41 as "silica source" for secondary synthesis with extending the reaction time of periods. Therefore, the pore wall thickness was increased systematically by extending the time. The remarkable stability is attributed to the combination of thicker pore walls and less strained silica frameworks.

J. Zhang et al., *Photocatalysis*, Lecture Notes in Chemistry 100,
https://doi.org/10.1007/978-981-13-2113-9_3

In general, developing new mesoporous structure, developing new synthetic methods, improving the crystallinity based on maintaining the structure, and seeking to optimize the functional structure and so on will continue to be hot spots for researchers in the future.

3.2 The Development of Mesoporous TiO_2 in Photocatalysis

3.2.1 The Preparation of Mesoporous TiO_2

Highly efficient mesoporous TiO_2 materials have been applied to the development of the sustainable, nonhazardous, and economical processes in different reaction systems and conditions (Fig. 3.1). It can be utilized in purification of polluted water and air, the decomposition of H_2O into H_2 and O_2, self-cleaning, and so on [5]. Currently, there are various preparation techniques of mesoporous titanium dioxide, such as sol–gel method [6–9], hydrothermal synthesis [10–14], atmospheric liquid phase [15], and radio frequency magnetron sputtering deposition method [16–19]. In addition to these methods, the removal of template for mesoporous titanium dioxide is also available now [20–24].

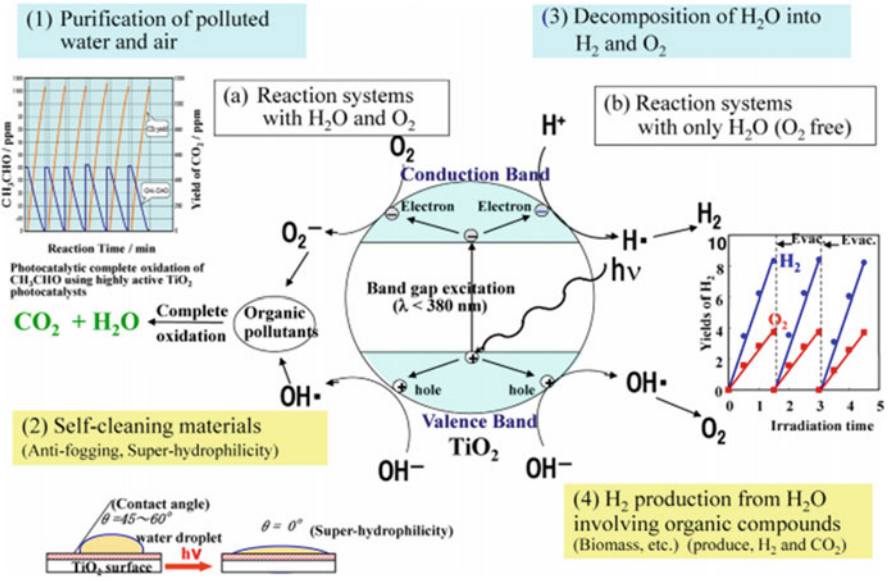

Fig. 3.1 (**a**) Applications of titanium oxide-based photocatalysts in the reaction system with H_2O and O_2. (**b**) Reaction systems with only H_2O (O_2 free). Inserted figure shows the production of electrons in the conduction band and holes in the valence band under UV light irradiation of TiO_2 semiconducting materials. (Reprinted with permission from Ref. [13].Copyright 2000, Royal Society of Chemistry)

Regarding the synthetic methods discussed above, we have listed some advantages and disadvantages among them. Sol–gel method exhibits good properties in terms of synthesized materials, such as low cost, high purity, good uniformity, and easy to be doped. In this part, organic and inorganic titanium precursors can be used to obtain photocatalysts, for example, TTIP and $TiCl_4$. Hydrothermal methods can prepare materials with high crystallinity; meanwhile, it can save time. In this method, there are various options of titanium precursors, such as $TiOSO_4$, TBOT, and TTIP. Compared with the previous two synthesis methods, the advantage of atmospheric liquid phase method is that it merely requires simple experimental equipment; thus it can achieve the possibility of industrialization. Adding the template agent during the reaction, and then stripped by heating or other methods to remove template, is a general method for the preparation of mesoporous materials. As a result, the heat treatment will significantly influence the products' structures, and inorganic skeleton is prone to collapse. Additionally, this process takes several hours, greatly extends the reaction time, and increases energy consumption. Hence, the adverse effect of template removal method is obvious. Moreover, the experimental conditions are not only harsh but also cumbersome. As to the radio frequency magnetron sputtering deposition method (RF-MS), the general way is using the TiO_2 plate, and then the depositions are carried out in a mixture of Ar and O_2. The thin films can be deposited on metal substrates such as Al, Fe, Ti, Zr, Pd, and Pt. Analyzing these methods, it is interesting to find the samples prepared by RF-MS methods have much smaller BET areas than those samples prepared by other three methods; therefore, each kind of catalysts has unique applications owing to their special properties.

3.2.2 Doping Modification on Mesoporous TiO_2

Since the discovery of mesoporous silica M41S, a variety of mesoporous materials have been synthesized [2]. These mesoporous materials exhibit widely potential applications in the industrial catalytic reactions, because they have high surface area, large pore size, and multidimensional framework and they are easy to be recycled. However, the widespread technological use of mesoporous TiO_2 is always to some extent constrained by its wide bandgap (3.2 eV), which requires ultraviolet irradiation for photocatalytic activation. And TiO_2 only absorbs 5% of the spectrum of the sunlight in the near ultraviolet region, which greatly limits its efficient application. To achieve efficient photocatalytic activity in the visible light range, one strategy is to reduce the bandgap of TiO_2. Doping of metal and nonmetal elements seems to be an effective method to enhance the photoactivity of mesoporous TiO_2.

In 2001, the metal ion implantation of TiO_2 with metal ions (V^+, Mn^+, Fe^+) at high energy acceleration was prepared by Yamashita et al. [25]. These catalysts exhibited photocatalytic reactivity for degradation of 2-propanol diluted in water under visible light irradiation ($\lambda > 450$ nm). After then, Zhang et al. [10] obtained the large mesoporous microspheres of titania and WO_3/TiO_2 composites by using $TiOSO_4$ as an inorganic precursor and P123 as structure directing agent via

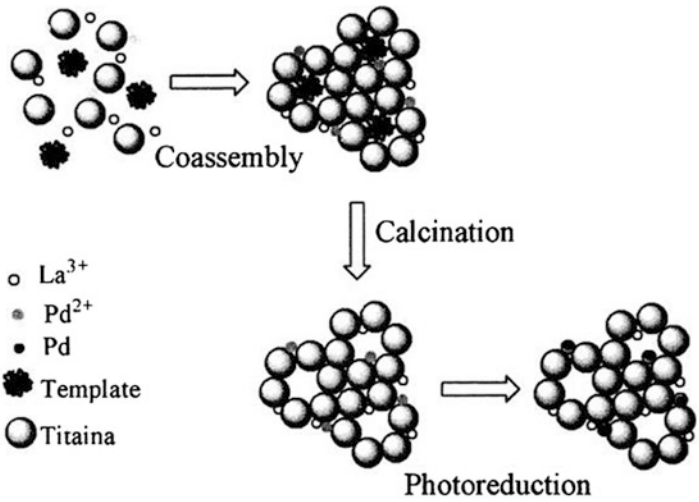

Fig. 3.2 Preparation of Pd nanoparticles in La-doped mesoporous titania by co-assembly and in situ photoreduction. (Reprinted with permission from Ref. [28]. Copyright 2006, Springer)

hydrothermal route. The workers also evaluated its photoactivity by the degradation of methyl orange, which is representative of stable azo dyes. Moreover, Tian et al. [26] synthesized gold loaded on TiO_2 (Au/TiO_2) catalysts using Au (I)–thiosulfate complex $(Au(S_2O_3)_2)^{3-}$ as the golden precursor for the first time, and its photoactivity was tested by the degradation of MO under visible light. Also, Yuan et al. [27] reported that La^{3+}-doped mesoporous TiO_2 with a highly crystallized framework and long-range order was prepared by using nano-anatase particles as nano-building units. Based on the previous work [12], Yuan and his coworkers also prepared highly dispersed Pd nanoparticles in La-doped mesoporous TiO_2 with crystalline framework via co-assembly and photoreduction method [28] in 2006. Figure 3.2 is an illustration of the process. By using this simple method, highly dispersed Pd nanoparticles were prepared in La-doped mesoporous titania with crystallized walls by in situ photoreducing of PdO at room temperature.

In 2010, Zhang et al. [29] prepared Fe^{3+}-doped mesoporous TiO_2 with ordered mesoporous structure via the solvent evaporation-induced self-assembly process through using P123 as soft template. They also successfully prepared the copper impregnated Ms-TiO_2 by using water immiscible room-temperature ionic liquid 1-butyl-3-methyl-imidazolium-tetrafluoroborate as a template and an effective additional solvent via the sol–gel method at low temperature [30]. As a result, the photoactivity of the sample Cu/Ms-TiO_2 is superior to P-25, Ms-TiO_2, and 2.0% Cu/P-25 in the case of 2,4-dichlorophenol and methyl orange under visible light ($\lambda > 420$ nm).

Not only the doping of metal can improve the photocatalytic activity, but also the doping of nonmental element can achieve the same goal. A thermal stable SiO_2-doped mesoporous TiO_2 with high crystallinity was prepared through a templating

method proposed by Zhang et al. [31]. It was found that the 15% SiO_2-dopped mesoporous TiO_2 exhibited much higher photoactivity than P25, attributing to the high anatase crystallinity, large specific surface area, abundant preserved surface hydroxyl groups, and mesoporous channels. In 2010, N and F co-doped TiO_2 microspheres were prepared by ethanol solvothermal method, using tetrabutyl titanate as precursor, urea as a nitrogen source, and ammonium fluoride as a fluorine source [32]. Then Zhang and his group reported that the synergetic effect of nitrogen and fluorine doping is responsible for the enhancement of photodegradation activity of AO7 under the irradiation of visible light. Later, Zhang et al. [33] synthesized N, B, Si-tridoped mesoporous TiO_2 photocatalyst through a modified sol–gel method. In this process, dodecylamine not only acted as a pore template but also as a nitrogen dopant, and H_3BO_3 acted as a boron dopant. Moreover, it showed a strong absorption in the visible light region because the doping of N and B narrowed the bandgap.

Besides doping of either metal or nonmental elements, the co-doping of metal and nonmetal element is another effective way of modification. For instance, Zhang et al. [34] obtained the iron (III) and nitrogen co-doped mesoporous TiO2 for the first time by the modified sol–gel method. Ma et al. [35] synthesized well-ordered mesoporous TiO_2 co-doped with nitrogen and ytterbium by an evaporation-induced self-assembly process.

The merits of mesoporous TiO_2 have been listed aforementioned. And we have summarized various preparation methods reported in existing literature as well. By doping modification of TiO_2, the photoactivity of corresponding catalysts can be enhanced to some extent; however, the fast recombination of electron–hole pairs and scarce adsorptive sites undermined the further research. According to some reported literatures, the composition of Si or porous MOFs with the TiO_2 may be a feasible way in enhancing the separation of electrons and holes.

3.2.3 Mesoporous TiO_2–Graphene Materials

Graphene (GR) possesses large specific surface area, excellent conductive, mechanical, and hydrophobic properties, which allow it to be multifunctional materials with excellent capacity for carrying and conducting electrons and holes. Especially, three-dimensional (3D) graphene aerogels (GAs) compounded with mesoporous TiO_2 composites are ultralight massive catalysts, which display hydrophobic properties and facilitate photocatalytic recyclings. In 2014, Qiu et al. [36] studied TiO_2–graphene composites as solar light photocatalysts and electrode materials for lithium–ion batteries (LIBs). They used a one-step hydrothermal method to prepare 3D-structured TiO_2/GA composites. In this process, $Ti(SO_4)_2$ was firstly dissolved in aqueous solution to form crystal seeds before a known amount of glucose was adsorbed on the seeds, followed by fixation of the seeds on the surface of graphene oxides. The presence of glucose results in the exposure of (001) facets in the nanocrystals up to 50% (inset of Fig. 3.3b), achieving the sizes ranging from 15 to 20 nm and realizing mesoporous interface between TiO_2 and the GR (in Fig. 3.3c).

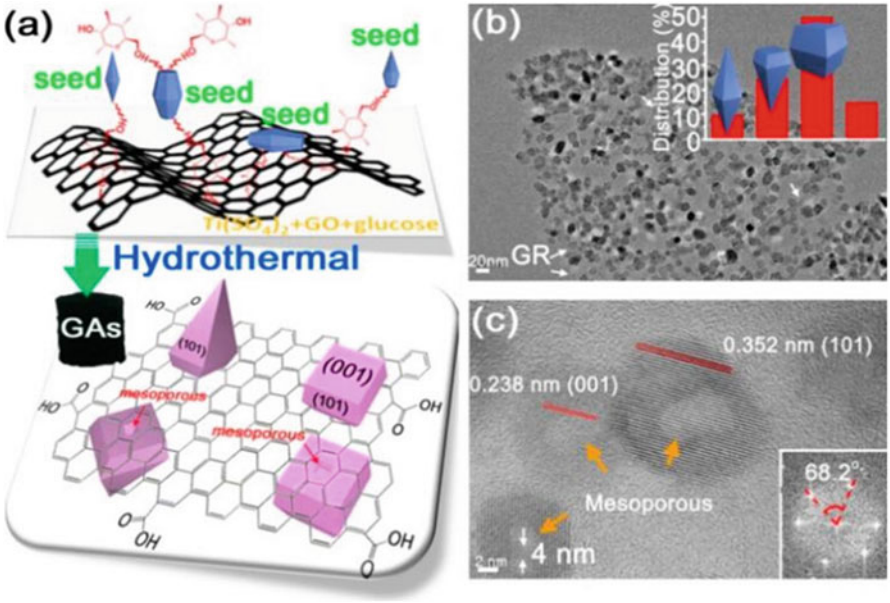

Fig. 3.3 (**a**) Glucose-linked transformation pathway for the in situ growth of TiO_2 nanocrystals with (001) facets on the GAs surface. (**b**) TEM image for TiO_2/GAs (67 wt % of TiO_2 in TiO_2/GAs). Inset (b) is the corresponding morphology distribution of the TiO_2 nanocrystals derived from 100 of TiO_2 crystals in image (**b**). (**c**) HRTEM image for TiO_2/GAs (67 wt %). Inset (**c**) is the corresponding fast Fourier transform (FFT) pattern. (Reprinted with permission from Ref. [36]. Copyright 2014, American Chemistry Society)

3.3 The Development of TiO_2–SiO_2 Mesoporous Materials

In this section, we briefly introduce the research of TiO_2–SiO_2 mesoporous materials. Although TiO_2 has some important properties, for instance, nontoxicity and excellent photostability, there are also some drawbacks constraining the performance of TiO_2 in photocatalytic process [37, 38]. To overcome the drawbacks, the researchers have prepared TiO_2 compounded materials that can provide large number of adsorptive sites by dispersion of TiO_2 species into a porous support with large surface area. Silica has been widely employed as the carrier, owing to its outstanding mechanical strength, high inner surface area, and uniform pore size. With the highly dispersion of TiO_2 into the porous SiO_2 support, the TiO_2–SiO_2 mixed oxide photocatalysts have shown significantly enhanced activities compared to pure TiO_2. On the one hand, TiO_2 and SiO_2 may be combined together to form a mixture of the two oxides, with interaction forces other than weak Vander Waals forces. On the other hand, they can integrate by means of the formation of Ti–O–Si bonds to form the composite oxides. When combined together through chemical bonding, the physical–chemical properties of TiO_2–SiO_2 differ from simple combination of each phase. In a word, homogeneity or dispersion largely depends on preparation methods

and synthesis conditions. Those novel TiO_2–SiO_2 materials not only take advantages of both TiO_2 (an n-type semiconductor and an active catalytic support) and SiO_2 (high thermal stability and excellent mechanical strength) but also extend their applications through the generation of new catalytic active sites based on the interactions between TiO_2 and SiO_2 [39]. Hence, it is indeed a promising and new catalytic material in many research areas.

3.3.1 The Preparation of TiO_2–SiO_2 Mesoporous Materials

There are various methods of preparing TiO_2–SiO_2 mesoporous materials, such as sol–gel method [38, 40–42], hydrothermal method [43, 44], chemical vapor deposition [45], precipitation method [46], liquid phase deposition [47], microwave irradiation method [48], impregnation method [49, 50], and evaporation-induced self-assembly (EISA) method [51].

For instance, TiO_2–SiO_2 nanocomposite can be prepared by sol–gel method. Commonly, the first step is to formulate sol with all kinds of ingredients, and then the gelation process, and at last removal of the surfactant to obtain mesoporous materials. In 2003, titania–silica mixed oxides were prepared by the sol–gel method from tetraethylorthosilicate (TEOS) and titanium (IV) isopropoxide (TTIP) as precursors by Elizabeth et al. [42]. Li et al. [43] also obtained silica-modified titanium dioxides by a hydrothermal method. There was strong interaction between SiO_2 and TiO_2, and Ti–O–Si bonds formed during the hydrothermal process. In addition, He et al. [51] synthesized highly ordered bicontinuous cubic mesoporous titania–silica binary oxides via an evaporation-induced self-assembly (EISA) method. As illustrated in Scheme 3.1, TTIP and TEOS hydrolyzed simultaneously with the existence of HCl, then the condensation and polymerization of TTIP were slowed down, and later the hydrolysis of TEOS was accelerated owing to the large amount of HCl. In the aging section, titanium species and silica species co-assembly with F127, and ordered mesostructures were formed. In the calcination process, titanate oligomers and silicate oligomers can be cross-linked with each other through the Ti–O–Si bonds. Under this circumstance, silica acts as glue between TiO_2 nanocrystals; thus, the thermal stability of the mesostructures can be improved. Moreover, Li et al. [49] successfully introduced benzopyrylium salt S-2(2,4-diphenyl-5,6,7,8-tetrahedro-1-benzopyrylium perchlorate) into the channels of mesoporous molecular sieves Ti-HMS with different Ti content by impregnation method.

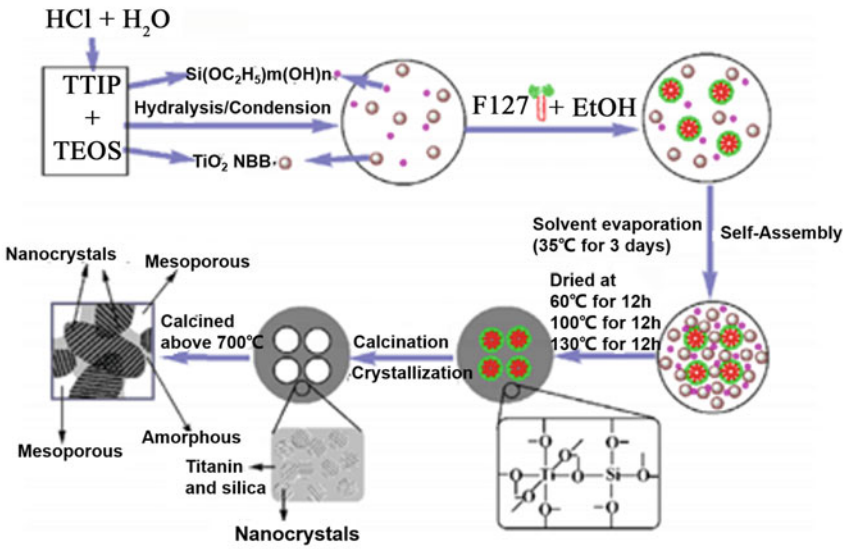

Scheme 3.1 Illustration for the self-assembly and structure evolution process of mesostructured titania–silica binary oxides. (Reprinted with permission from Ref. [50]. Copyright 2005, Elsevier)

3.3.2 The Application of TiO_2–SiO_2 Mesoporous Materials in Photocatalysis

3.3.2.1 Photodegradation of Organic Pollutants

We have briefly introduced the preparation methods of TiO_2–SiO_2 mesoporous materials. Next, we will explore its applications. As we all know, human's demand of energy will be much greater by the year of 2050. This increase poses an undue burden to our environment and the length of human's life. Besides that, with the prosperity of industrialization, the disposal of industrial waste poses a great threat to the environment, which is becoming the biggest concern for the sustainable development of human society. As previously mentioned, TiO_2 was considered as a catalyst for degradation lots of pollutants. However, its rapid recombination of photo-generated electron–hole pairs limits its application. According to previous reports, TiO_2–SiO_2 mesoporous materials are found to be effective in environmental remediation. Figure 3.4 briefly demonstrates the photocatalytic process of degradation of organic pollutants and dyes under visible light [52].

Aguado et al. [53] prepared titania-supported sample on different types of silica through a sol–gel method followed by hydrothermal processing. Afterward, the catalysts were tested by the degradation of iron (III) cyano complexes. In all cases, photoinduced CN^- released from the composite which happened by a homogeneous process. He et al. [59] applied cubic mesoporous titania–silica binary oxides to

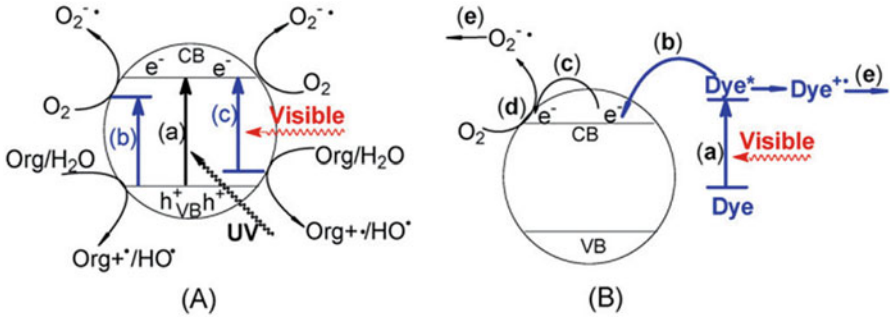

Fig. 3.4 Strategies to realize visible light-induced degradation of organic pollutants on a semiconductor with a wide bandgap. (**a**) The band–band excitation of the pure semiconductor under UV irradiation (*a*) and the bulk-doping to extend the photoresponse by forming electronic states below the conduction band (*b*) or above the valence band (*c*) of the semiconductor in the bandgap. (**b**) The semiconductor-mediated photodegradation initiated by the surface electron injection from the adsorbed dye molecular that harvest visible light. (Reprinted with permission from Ref. [51]. Copyright 2009, Elsevier)

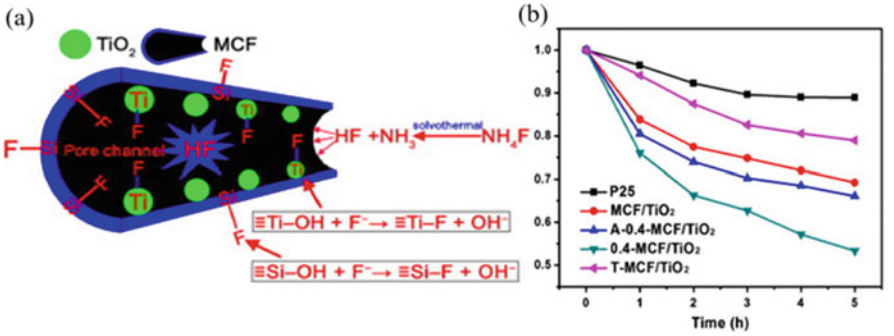

Fig. 3.5 (**a**) Illustration of the fluorination reaction occurred in the pore channels of MCF; (**b**) visible light photocatalytic activities of different samples. (Reprinted with permission from Ref. [53]. Copyright 2002, Elsevier)

degrade rhodamine B (RhB) under UV light irradiation. The result shows that the sample has a comparable photocatalytic activity with Degussa P25, and higher activity than pure TiO_2.

In terms of MCF materials, some papers have reported about it. Xing et al. [44] have obtained super-hydrophobic mesocellular foam (MCF), which is loaded with nano-sized TiO_2 photocatalysts in its pore channels, through a simple one-step solvothermal method followed by a low-temperature vacuum activation process to produce Ti^{3+}. And it can be well considered as an extractant for organics. In this method, NH_4F is used as hydrophobic modifier, and isopropanol is used as solvent to synthesize the super-hydrophobic mesoporous MCF loaded with highly dispersed and Ti^{3+} self-doped TiO_2 nanoparticles. Figures 3.5a illustrates the fluorination reaction occurred in the channels of MCF. In comparison with fluorine-containing

silylation organic agent, NH_4F is easy to release HF during solvothermal process. And F ions will be adsorbed onto the MCF under acidic conditions owing to its mesoporous structure. TiO_2 particles are deposited into MCF's pore channels, indicating that the exchange between surface hydroxyl groups on TiO_2 and F ions to form the Ti–F bonds is effectively promoted. Simultaneously, the F ions adsorbed in channels also replace the surface hydroxyl groups on SiO_2 to generate the Si–F bonds. Ti^{3+} was generated in the vacuum drying process, which plays an important role in enhancing its visible light photocatalytic activity. During the degradation of RhB, the NH_4F-modified catalyst of 0.4-MCF/TiO_2 exhibited the optimal photocatalytic activity, indicating that the NH_4F modification and vacuum activation are beneficial to improving visible light photoactivity (Fig. 3.5b).

3.3.2.2 Water Splitting

Since the initial photocatalyst for water splitting into hydrogen and oxygen was developed in 1972 [54]. Various semiconductor-based catalyses either using UV or visible light have been investigated. As discussed in the above section, TiO_2–SiO_2 composite materials, which are combined with each other physically as well as chemically, can enhance photocatalytic activity; thus, these materials attracted much attention. In recent years, scientists deduced new two-step photoexcitation processes, the so-called Z-scheme [55], in order to realize overall water splitting (Fig. 3.6). This system consists of two visible light responsive semiconducting photocatalysts (A and B) and a redox mediator. Photocatalyst A is responsible for hydrogen evolution which is excited by visible light, and then, photo-formed electrons reduce H^+ into H_2 together with photo-formed holes oxidizing the redox

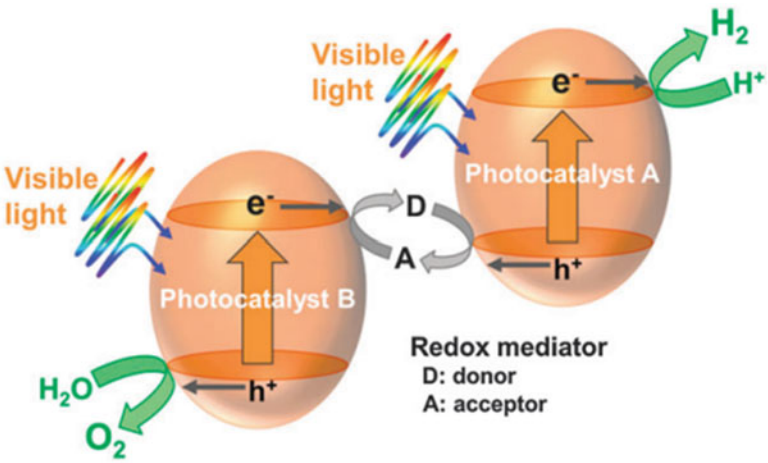

Fig. 3.6 Conceptual diagram of a Z-scheme photocatalytic system. (Reprinted with permission from Ref. [55]. Copyright 2013, Royal Society of Chemistry)

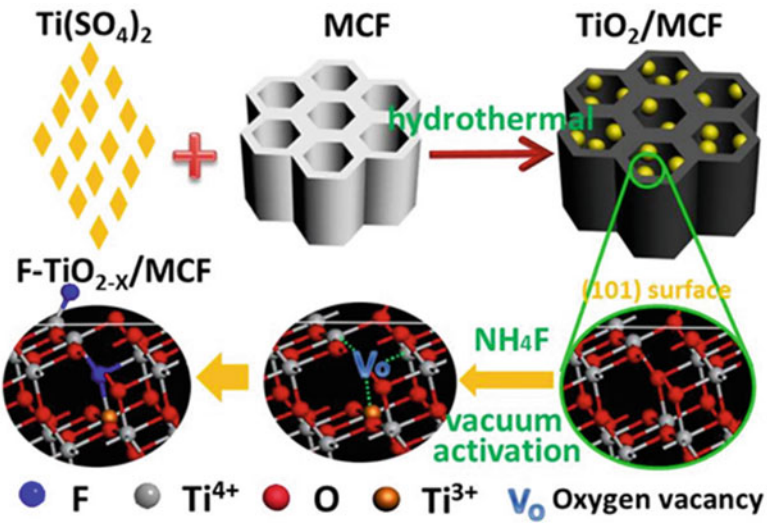

Scheme 3.2 Synthetic steps for the production of the fluorine-doped TiO_{2-x}/MCF composite and the displacement of lattice oxygen vacancies with F atoms during vacuum activation. (Reprinted with permission from Ref. [57]. Copyright 2014, Wiley)

mediator. At the same time, photocatalyst B is used for the water-oxidation reaction, during which photo-formed holes oxidize H_2O to produce O_2 together with photo-formed electrons reducing the redox mediator under visible light irradiation. Finally, water splitting into H_2 and O_2 is attained.

Niphadkar et al. [56] prepared TiO_2–SiO_2 mesoporous composite photocatalysts with different proportions of TiO_2 and SiO_2 by loading TiO_2 on as-synthesized Si–MCM-41 using simple sol–gel method. The photocatalytic evaluation of composite photocatalysts was carried out in production of hydrogen by water-splitting reaction under UV light. In 2014, Xing et al. [57] successfully prepared a brown mesoporous TiO_{2-x}/MCF composite with a high fluorine doping concentration (8.01 at%) by vacuum activation method. It displays an excellent solar absorption, a record-breaking quantum yield ($\Phi = 46\%$) and a high photon–hydrogen energy conversion efficiency ($\eta = 34\%$) in solar photocatalytic H_2 production process, which are all better than that of the black hydrogen-doped TiO_2 ($\Phi = 35\%$, $\eta = 24\%$). Scheme 3.2 illustrates the continuous steps for preparing F-TiO_{2-x}/MCF. Firstly, titanium source Ti $(SO_4)_2$ in situ transformed to TiO_2 nanocrystals in the pore walls of the MCF through hydrothermal method. Then NH_4F was added into the solution, mechanically mixed with the obtained TiO_2/MCF, followed by a vacuum activation treatment to produce oxygen vacancies in TiO_2 and the substitution of fluorine atoms for vacancies. The F-TiO_{2-x}/MCF exhibits much higher rate of H_2 generation than black H-TiO_{2-x}, P25 and other photocatalysts (Fig. 3.7a). In addition to H_2 evolution, the solar light, UV light, and visible light-driven photodegradation of dyes by F-TiO_{2-x}/MCF were also measured. It was shown that catalysts treated by vacuum activation exhibited better photocatalytic activity than the blank samples (Fig. 3.7b).

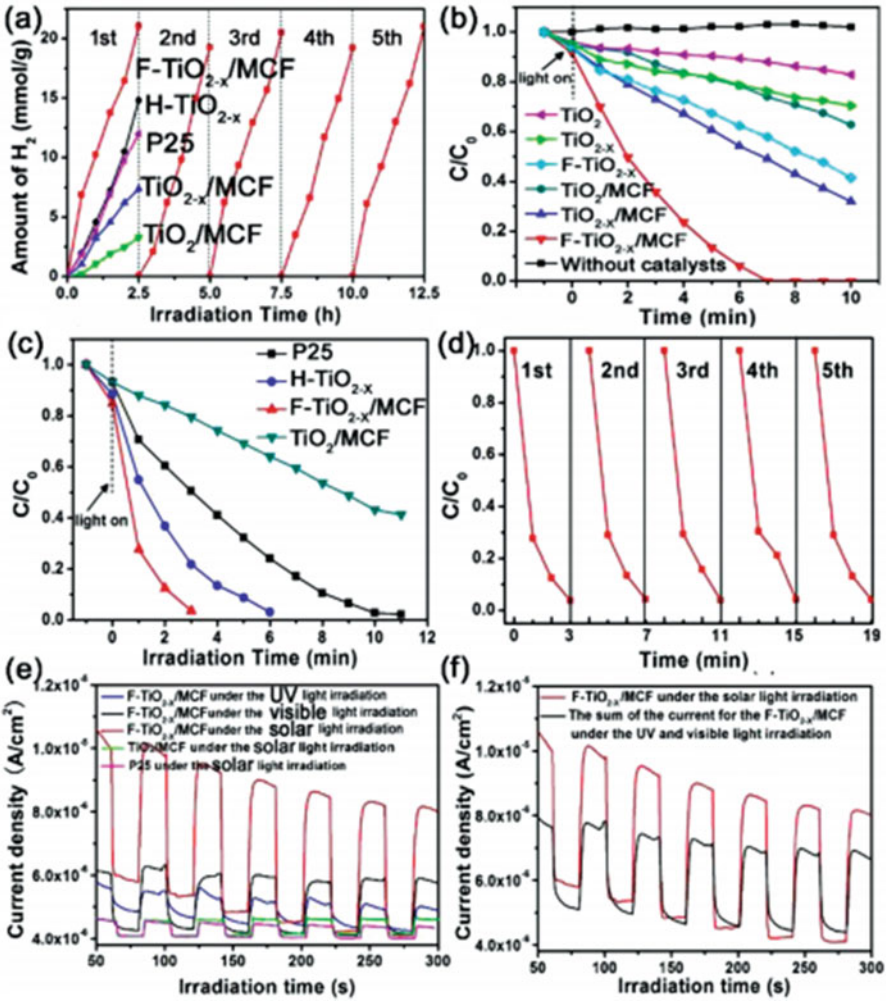

Fig. 3.7 (**a**) Solar light-driven (with an AM 1.5 air mass filter) photocatalytic water splitting for H_2 generation and the cycling measurements of F-TiO_{2-x}/MCF; (**b**) photocatalytic activities for degradation of MO induced by simulated solar light; (**c**) a comparison of photocatalytic decomposition of MB by F-TiO_{2-x}/MCF, blank H-TiO_{2-x}, and other catalysts under simulated solar light irradiation (with an AM 1.5 air mass filter); (**d**) cycling tests of solar-driven photocatalytic activity of F-TiO_{2-x}/MCF for the degradation of MB; (**e**) transient photocurrent responses of F-TiO_{2-x}/MCF in 0.5 M Na_2SO_4 aqueous solution under various irradiation conditions (UV light, < 380 nm filter; visible light, > 420 nm filter); (**f**) comparison between the solar light-driven photocurrent and the sum of the photocurrent of F-TiO_{2-x}/MCF under UV and visible light irradiation. (Reprinted with permission from Ref. [57]. Copyright 2014, Wiley)

To investigate the photoactivity of brown F-TiO_{2-x}/MCF, F-TiO_{2-x}/MCF, and hydrogen-doped TiO_2 (H-TiO_{2-x}), these samples were measured for the degradation of methylene blue (MB) under simulated solar light irradiation using an AM 1.5 air

mass filter (Fig. 3.7c). What is more, cycling tests revealed that the brown F-TiO_{2-x}/MCF sample is especially stable after five photocatalytic cycles (Fig. 3.7d). The F-TiO_{2-x}/MCF was shown to produce electrons and exhibit a much higher photocurrent response than MCF/TiO_2 under solar light irradiation. Its solar light-driven current density is much higher than its UV and visible light-driven density as well (Fig. 3.7e). It is worth noting that the solar light-driven current density of F-TiO_{2-x}/MCF is much higher than the sum of the current densities of the catalyst under UV and visible light irradiation (Fig. 3.7f), which indicates that the lifetime of solar light-produced electrons exceeds those of UV- or visible light-produced electrons. It was concluded that the decrease of recombination sites induced by high concentration F doping and the synergistic effect between lattice Ti^{3+}-F and surface Ti^{3+}-F are responsible for the excellent absorption of solar light and photocatalytic production of H_2 of these catalysts.

In this section, we firstly introduce the application of mesoporous TiO_2–SiO_2 materials. It can be either applied to photodegradation of pollutants or used for hydrogen production. Then, we have briefly listed some notable literatures and analyzed them.

3.4 Visible Light Response Metal–Organic Frameworks (MOFs)

In recent years, visible light responsive porous metal–organic framework photocatalysts have been investigated deeply. Metal–organic frameworks (MOFs) are hybrid materials composed of organic linkers and metal–oxo clusters. These MOF materials are hot spots in research, and it can be utilized as adsorbents, separation materials, ion-conductive materials, and catalysts. Among various highly porous materials, metal–organic frameworks (MOFs) are unique in their degree of tunability, structural diversity, as well as their range of chemical and physical properties. Metal–organic frameworks (MOFs) are also known as coordination polymers, which are crystalline materials generated by the association of metal ions (nodes) and multitopic organic ligands (rods) [58–61]. Based on their structures, MOFs have been considered as a promising type of materials due to its unique attributes and open structures with periodic dual composition, which is amenable to bottom up assembly of secondary building blocks into a desired framework expanding or decorating a specific blueprint network topology [58, 62]. As a kind of porous material, metal–organic frameworks (MOFs) have shown semiconductor-like characteristics in photocatalysis [63–67]. In 2009, Kataoka et al. [67] have detected the first example of open porous metal–organic frameworks (MOFs) that functions as an activity site for the reduction of water into hydrogen molecules in the presence of $Ru(bpy)_3^{2+}$,MV^{2+}, and EDTA–2Na under visible light irradiation. Also, Zhou et al. [63] have synthesized and characterized a new metal–organic framework (MOF-253-Pt) material through immobilizing a platinum complex in 2,20-

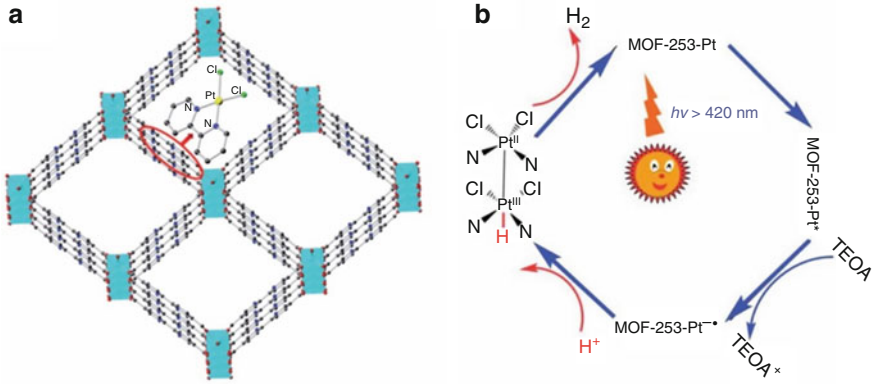

Fig. 3.8 (**a**) Model structure of MOF-253-Pt, through post-synthetic modification of MOF-253 with $PtCl_2$. Key: Cyan octahedron represents Al atoms, while yellow, green, red, blue, and blank circles represent Pt, Cl, O, N, and C atoms, respectively; H atoms are omitted for clarity. (**b**) Proposed reaction mechanism for the photocatalytic H_2 evolution over MOF-253-Pt under visible light irradiation. (Reprinted with permission from Ref. [63]. Copyright 2013, Royal Society of Chemistry)

bipyridine-based microporous MOF (MOF-253) using a post-synthesis modification strategy. The functionalized MOF-253-Pt serves both as a photosensitizer and a photocatalyst for hydrogen evolution under visible light irradiation. The structure and proposed mechanism are presented as shown in Fig. 3.8a, b, respectively. Upon light irradiation, the MOF with the presence of TEOA firstly generates a one-electron-reduced species MOF*(3MLCT) and holes. And then, the MOF*(^{3}MLCT) species is reductively quenched to form MOF^- with the electrons stored on the bpy^- ligands. After that, the reduced MOF^- further forms a Pt(III)-hydride intermediate via a proton-coupled electron transfer (PCET). The intermediates contribute to the formation of the hydride-diplatinum (II, III) intermediate by the synergistic effect of the nearing anchored $Pt(bpy)Cl_2$ complex on framework, leading to H_2 production by a heterolytic coupling pathway.

In 2016, it has been discovered that improving the efficiency of electron–hole separation and charge-carrier utilization plays a central role in photocatalysis. Jiang et al. [68] prepared a representative metal–organic framework (MOF) UiO-66-NH_2, in which Pt nanoparticles of ca. 3 nm are incorporated inside or supported. The resulting products are denoted as Pt@UiO-66-NH_2 and Pt/UiO-66-NH_2, respectively. Finally, these materials are especially applied in photocatalytic hydrogen production via water splitting. Scheme 3.3 simply clarified the pathway of synthesizing these two different materials. Pt@UiO-66-NH_2 greatly shortens the electron-transport distance and hence suppresses the electron–hole recombination, which is expected to have an enhanced catalytic activity compared to Pt/UiO-66-NH_2. In addition, the Pt NPs embedded in the MOF do not undergo aggregation or leaching during the reaction, which leads to better catalytic recyclability of Pt@UiO-66-NH_2 than that of Pt/UiO-66-NH_2.

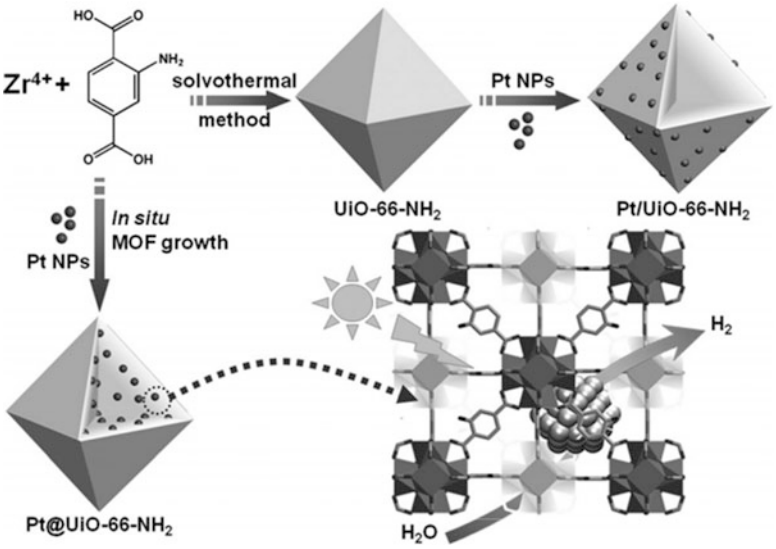

Scheme 3.3 Schematic illustration for the synthesis of Pt@UiO-66-NH_2 and Pt/UiO-66-NH_2, with the photocatalytic hydrogen production process over Pt@UiO-66-NH_2. (Reprinted with permission from Ref. [68]. Copyright 2016, Wiley)

In 2010, Garcia and his coworkers synthesized the Zr-containing metal–organic frameworks (MOFs) that exhibited photocatalytic activity for hydrogen generation upon irradiation at wavelength longer than 300 nm [69]. In 2012, Anpo et al. [64] employed 2-amino-benzenedicarboxylic acid as an organic linker to synthesize amino-functionalized Ti (IV) metal–organic framework (Ti–MOF–NH_2) by a facile solvothermal method, and it described the hydrogen production from an aqueous medium under visible light. The structure of the Ti–MOF–NH_2, its mechanism, and the yield of hydrogen are shown in Fig. 3.9. In summary, it is mentioned that Ti–MOF materials of semiconductor properties have potential in water splitting. All the reported literatures provide us with new ideas in the further development of water splitting.

With the exception of the application in water splitting, the Ti–MOFs can also be applied to CO_2 reduction. In the same year, Li et al. [70] successfully prepared a targeted photoactive catalyst $Ti_8O_8(OH)_4$(bdc-NH_2)$_6$ (NH_2-MIL-125 (Ti)) for the first time, which reduced CO_2 even under visible light irradiation. In Fig. 3.10a, MIL-125 (Ti) shows an absorption edge at 350 nm, whereas NH_2-MIL-125 (Ti) shows an extra absorption band in the visible light region with the absorption edge extending to around 550 nm, which is in agreement with the bright yellow color. An interesting photochromic phenomenon was observed over NH_2-MIL-125 (Ti) during the photocatalytic reaction. When the solution of NH_2-MIL-125 (Ti) and TEOA in MeCN was irradiated with visible light in the presence of N_2, the color of the solution changed from the original bright yellow to green. After CO_2 or O_2 was introduced into the reaction system, the green color of the solution changed gradually

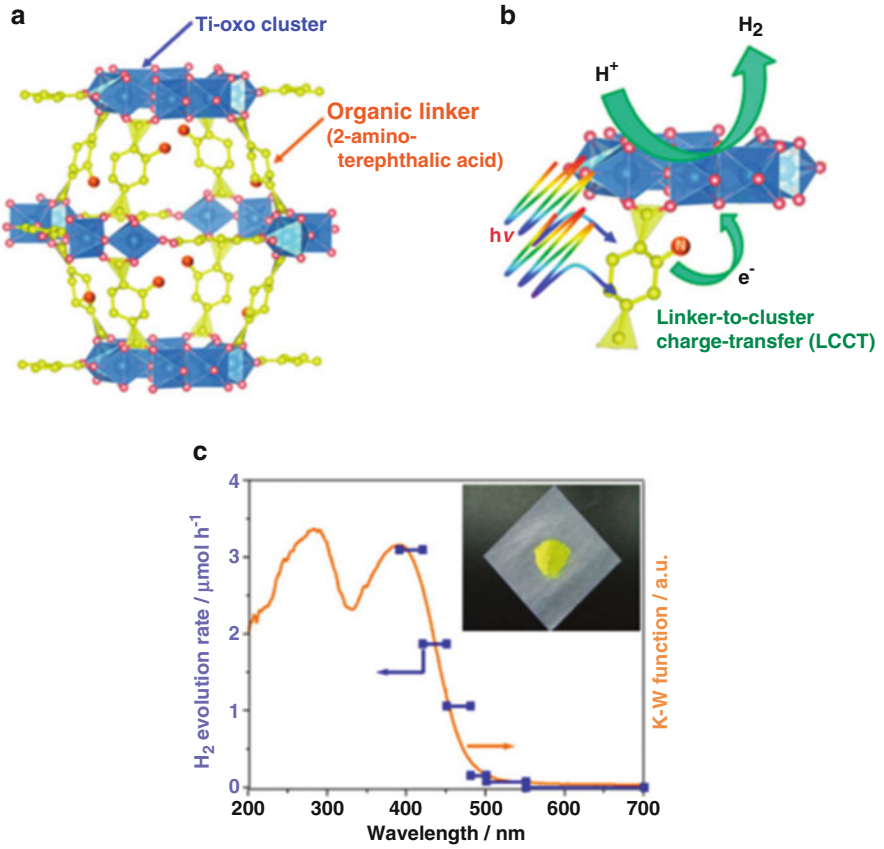

Fig. 3.9 Schematic illustrations of (**a**) the structure of Ti–MOF–NH_2 and (**b**) the reaction mechanism for hydrogen evolution over Ti–MOF–NH_2 induced by visible light irradiation. (**c**) Action spectrum for hydrogen evolution from water containing TEOA as a sacrificial electron donor over Ti–MOF–NH_2. Inset shows the photograph of Ti–MOF–NH_2. (Reprinted with permission from Ref. [64]. Copyright 2012, American Society Chemistry)

back to the original bright yellow (Fig. 3.10b). The photochromic phenomenon is ascribed to the presence of the inter-valence electron transfer from the optically induced hopping of electrons from Ti (III) to Ti (IV) sites in the titanium–oxo clusters.

Despite water splitting and CO_2 reduction, it was also reported by Garcia and Majima [71, 72] that the combination between the organic linkers and metal–oxo clusters would enable the development of dye-sensitized type MOF photocatalysts operating under visible light illumination. In 2012, Zhang et al. [73] adopted a doping strategy to tune the gas sorption and photocatalytic properties of a microporous material ZIF-67. It is worth mention that the Cu-doped phase integrated both structural

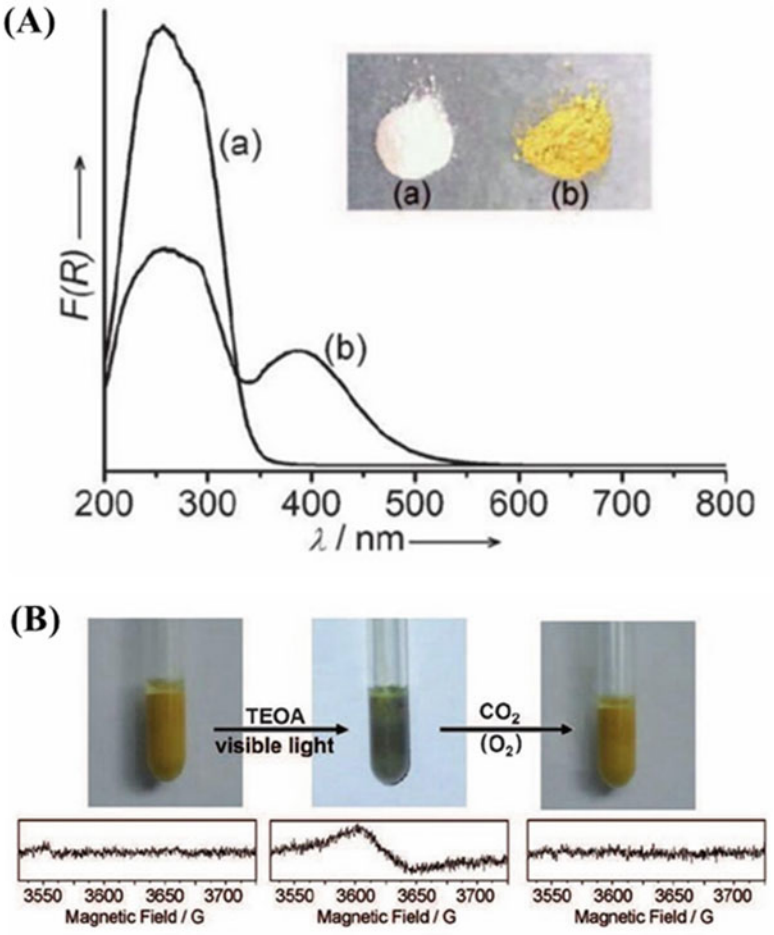

Fig. 3.10 (**a**) UV-vis spectra of (a) MIL-125(Ti) and (b) NH_2-MIL-125(Ti). The inset shows the samples. (**b**) Photos and corresponding ESR spectra of NH_2-MIL-125(Ti) under different conditions: (a) fresh NH_2-MIL-125(Ti), (b) TEOA, visible light, and N_2 and (c) after the introduction of CO_2 (or O_2). (Reprinted with permission from Ref. [70]. Copyright 2012, Wiley)

features and functions of ZIF-67 showed high gas uptake capacity and highly efficient visible light-driven photocatalytic property upon the degradation of methyl orange.

3.5 The Development of Mesoporous Ti–SiO_2 Materials in Photocatalysis

Up to now, we have grasped some points of TiO_2–SiO_2 mesoporous materials; however, the concept of Ti–SiO_2 materials is totally different from TiO_2–SiO_2 mesoporous materials because of its containing Ti-oxides species. In the pioneering

work of Honda and Fujishima [54], they obtained the photo-assisted production of H_2 and O_2 from water with a photoelectrochemical cell consisting of a Pt and TiO_2 electrodes under a small electric bias. Moreover, TiO_2 photocatalysts with incorporated Ti-oxide species anchored onto supports such as SiO_2, glass, and zeolite exhibited selective photoactivity. The Ti-oxide species prepared within the supports, for example, SiO_2, glass, and zeolite, have revealed a unique local structure as well as high selectivity in the oxidation of organic substances with hydrogen peroxide. Ti–Si binary oxide powders with a low TiO_2 content prepared by sol–gel methods have been reported to include the fourfold coordinated Ti-oxide species highly dispersed within the SiO_2 matrices, showing a unique and characteristic photocatalytic performance for the hydrogenation of unsaturated hydrocarbons with H_2O; the decomposition of NO into N_2, O_2, and N_2O; as well as the reduction of CO_2 with H_2O to produce CH_3OH and CH_4 under UV light irradiation [74–79]. Moreover, many reports have mentioned that the specific photocatalytic reactivity of those catalysts was much higher than that for TiO_2 powder, which may be attributed to the tetrahedrally coordinated titanium oxide moieties. Thus, we will discuss it comprehensively in this section.

3.5.1 The Preparation of Ti–SiO_2 Mesoporous Materials

Many reports have been published on preparation of Ti–SiO_2 mesoporous materials, such as ionized cluster beam (ICB) method [76, 80], ion-exchange method [79, 81], anchored on substrate [74, 78, 82, 83], CVD method [84], hydrothermal synthesis method [85], solvent evaporation method [86], and metal ion implantation [87].

3.5.2 The Application of Ti–SiO_2 Mesoporous Materials in Photocatalysis

3.5.2.1 CO_2 Photoreduction

In 1992, Anpo et al. [82] prepared highly dispersed titanium oxide anchored onto Vycor glass through a facile reaction between surface OH groups of Vycor and $TiCl_4$. It was investigated that the photoreduction of CO_2 with H_2O should be linked to the high reactivity of the charge-transfer excited state, i.e., $(Ti^{3+}\text{-}O^{-})^{*}$, owing to the presence of well-dispersed homogeneous titanium oxide species on the surface. Ti-MCM-41 and Ti-MCM-48 mesoporous zeolite catalysts synthesized by hydrothermal method exhibited high and unique photocatalytic reactivity for the reduction of CO_2 with H_2O to produce CH_4 and CH_3OH in the gas phase [74]. Keita Ikeue et al. [86] also prepared self-standing porous silica thin films with different pore structures by a solvent evaporation method. From 2002 to 2003, Anpo and his coworkers reported many works about photocatalytic reduction of CO_2 on

Ti-containing porous silica thin film [86, 88, 89]. Figure 3.11a shows the yields of products with the change of reaction time. The yields of CH_4 and CH_3OH in the photocatalytic reduction of CO_2 and H_2O on the Ti-oxides containing various porous materials are shown in Fig. 3.11b. They found that it is possible to determine a real quantum yield of the photocatalytic reduction of CO_2 with H_2O on tetrahedrally coordinated Ti-oxides. Ti-oxide was constructed within porous silica material, and its quantum yield could to be 0.3% at room temperature by the total number of photons absorbed by the catalyst.

3.5.2.2 NO/NO_2 Photoreduction

In 1985, Anpo et al. [77] carried out a research on photoluminescence studies of titanium oxide anchored onto porous Vycor glass. It is proposed that the photoluminescence quenching is closely associated with the electron transfer from the excited states of the catalyst to the added O_2 or N_2O molecules. In Fig. 3.12, it shows the comparison between the reduction of NO and the decomposition of CO_2. The structure of Ti-oxide single-site is presented on the left top of this picture. Similarly, the structure of TiO_2 particles is presented on the right bottom of this picture. The quantum yield of $CO_2 + H_2O \rightarrow CH_3OH + CH_4$ is much smaller than the decomposition of NO, due to its demanding of more configurations of co-adsorbed reactants involving six participating atoms [90]. In 1997, titanium oxide catalysts prepared within the Y-zeolite cavities via an ion-exchange method were reported by Anpo et al. [79], which exhibited high and unique photocatalytic reactivities for the decomposition of NO into N_2 and O_2. It was also found that the charge-transfer excited state of the titanium oxide species, $(Ti^{3+}\text{-}O^{-})^*$, plays a vital role in these unique photocatalytic reactions. Table 3.1 revealed the yields of the photo-formed N_2 and N_2O and its selectivity in the photocatalytic decomposition of NO. It is obvious that the efficiency and selectivity of the formation of N_2 strongly depend on the type of catalysts.

In 2000, Masato Takeuchi et al. [76] prepared transparent TiO_2 thin film photocatalysts on transparent porous Vycor glass (PVG) by an ionized cluster beam (ICB) method. These thin films worked with high efficiency as photocatalysts for the decomposition of NO into N_2, O_2, and N_2O under UV light irradiation at 275 K. When the film thickness increases, the photocatalytic reactivity decreases gradually. In 2004, Yamashita and Anpo [80] proposed a new concept of an ion beam technology using accelerated metal ions, a metal ion implantation, and an ionized cluster beam (ICB) (detailed schematic diagram is shown in Fig. 3.13a). The decomposition of NO into N_2, O_2, and N_2O can be occurred not only under UV light but also visible light, realizing the efficient use of solar beam energy. The samples were also characterized by XANES (as shown in Fig. 3.13b). It revealed the XAFS (XANES and FTEXAFS) spectra of the Cr ion–implanted TiO_2 powder catalyst. By analyzing on these spectra, we can tell that in the Cr ion–implanted TiO_2, the Cr ions are highly dispersed in the lattice of TiO_2 possessing octahedral coordination. These Cr ions are isolated and substitute the Ti^{4+} ions in the lattice positions of TiO_2.

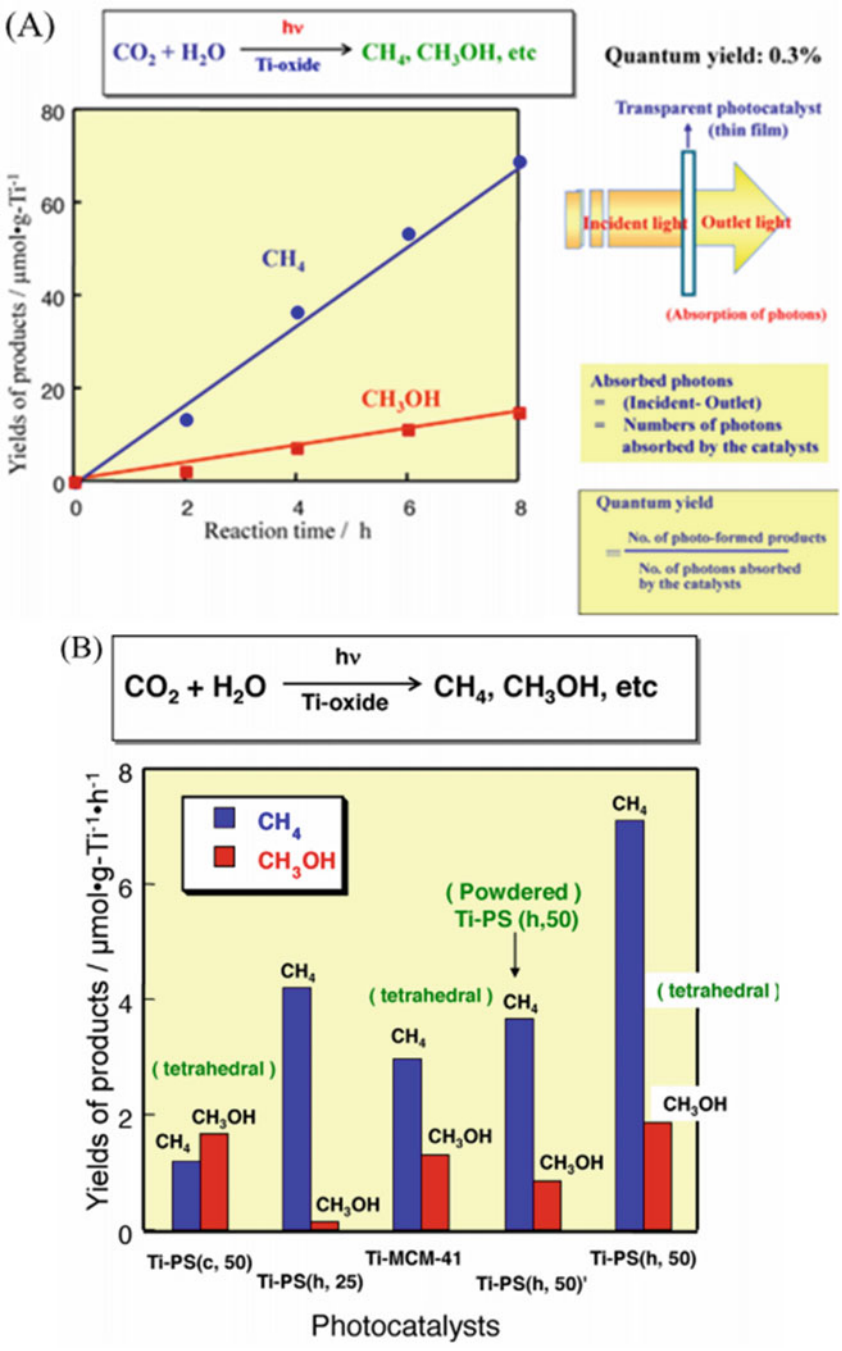

Fig. 3.11 (**a**) Reaction time profiles of the photocatalytic reduction of CO_2 with H_2O to produce CH_4 and CH_3OH on a Ti-oxide single-site containing mesoporous silica thin film photocatalyst at 298 K. Inserted figure shows how to measure the real quantum yields of the reaction. (**b**) The yields of CH_4 and CH_3OH in the photocatalytic reduction of CO_2 with H_2Oon Ti-PS (h, 25), Ti-PS(c, 50), Ti-MCM-41, powdered form of Ti-PS (h, 50) and Ti-PS (h, 50) photocatalysts at 295 K. (Reprinted with permission from [86, 88, 89]. Copyright 2002–2003, Elsevier)

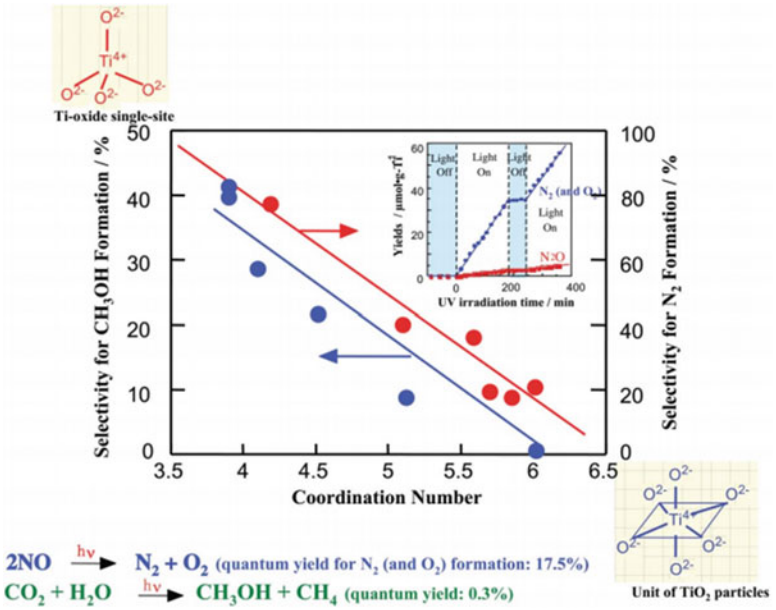

Fig. 3.12 Relationship between the coordination numbers and photocatalytic reactivity of titanium oxides. (Reprinted with permission from Ref. [78]. Copyright 1997, American Chemical Society)

Table 3.1 Comparisons of yields of N_2 and N_2O and their selectivities in the direct photocatalytic decomposition of NO at 275 K on various types of the Ti-oxide/zeolite catalysts and the powered bulk TiO_2 catalyst

Catalysts	Ti content (wt% of as TiO_2)	Yields (μmol/g-catalh)			Selectivity (%)	
		N_2	N_2O	total	N_2	N_2O
ex-Ti-oxide/Y-zeolite	1.1	14	1	15	91	9
imp-Ti-oxide/Y-zeolite	1.0	7	10	17	41	59
imp-Ti-oxide/Y-zeolite	10	5	22	27	19	81
Powered TiO_2	100	2	6	8	25	75

Besides that, the Cr-doped TiO_2 catalysts chemically prepared by impregnation or sol–gel method were found to have a mixture of the aggregated Cr-oxides in tetrahedral coordination similar to CrO_3 and octahedral coordination similar to Cr_2O_3.

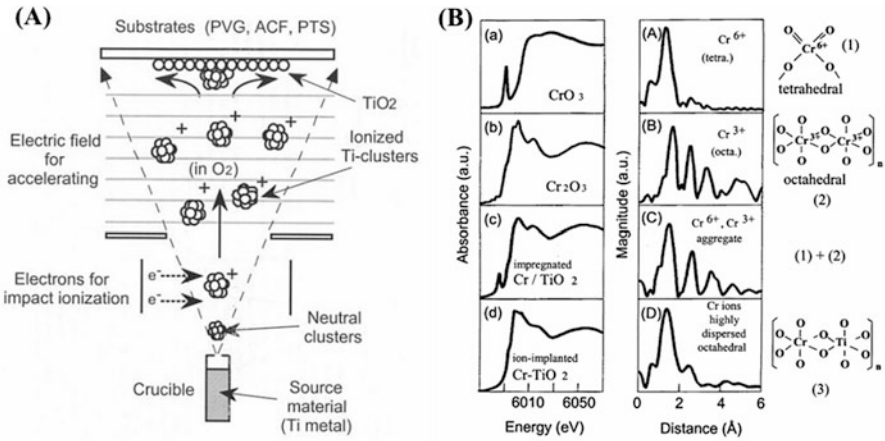

Fig. 3.13 (**a**) Schematic diagram of an ICB method. (**b**) XANES (a–d) and Fourier transforms of EXAFS (A–D) spectra of CrO_3 (A), Cr_2O_3 (B) and the Cr-impregnated TiO_2 (C) and Cr ion–implanted TiO_2 after calcination at 723 K (D). (Reprinted with permission from Ref. [81]. Copyright 2006, Springer)

3.6 Conclusion

Herein, to sum up, we have reviewed plenty of representative literatures about recent advances in photocatalysts over the highly dispersed TiO_2 in mesoporous materials. Although TiO_2 possesses specific properties, it is limited in photocatalysis because of its narrow bandgap. Thus, the doping modification on mesoporous TiO_2 materials proves to be an effective way to enhance its photocatalytic performance. Meanwhile, synthesizing mesoporous TiO_2–SiO_2, Ti–MOFs, and Ti–SiO_2 materials is another feasible way to achieve this goal. Based on the analysis of mechanism of these systems, it gives the researchers a promising future. The achieved progress in this field indicates that researchers can either be able to extend the photoresponse to the visible region or apply them to practical application, such as water splitting, degradation of pollutants and decomposition of greenhouse gas (CO_2, NO, NO_2).

References

1. Yuan S, Chen Y, Shi L, Fang J, Zhang J, Zhang J, Yamashita H (2007) Synthesis and characterization of Ce-doped mesoporous anatase with long-range ordered mesostructure. Mater Lett 61(21):4283–4286
2. Beck JS, Vartuli JC, Roth WJ, Leonowicz ME, Kresge CT, Schmitt KD, Chu CTW, Olson DH, Sheppard EW (1992) A new family of mesoporous molecular sieves prepared with liquid crystal templates. J Am Chem Soc 114(27):10834–10843
3. Ryoo R, Jun S (1997) Improvement of hydrothermal stability of MCM-41 using salt effects during the crystallization process. J Phys Chem B 101(3):317–320

4. Mokaya R (2001) Hydrothermally stable restructured mesoporous silica. Chem Commun 10(10):933–934
5. Anpo M (2013) Photocatalytic reduction of CO_2 with H_2O on highly dispersed Ti-oxide catalysts as a model of artificial photosynthesis. J CO2 Util 1:8–17
6. Antonelli DM, Ying J (1995) Synthesis of hexagonally packed mesoporous TiO_2 by a modified sol-gel method. Angew Chem Int Ed 34(18):2014–2017
7. Yang P, Zhao D, Margolese DI, Chmelka BF, Stucky GD (1998) Generalized syntheses of large-pore mesoporous metal oxides with semicrystalline frameworks. Nature 396 (6707):152–155
8. Zhang M, Bando Y, Wada K (2001) Sol-gel template preparation of TiO_2 nanotubes and nanorods. J Mater Sci Lett 20(2):167–170
9. Shibata H, Ogura T, Mukai T, Ohkubo T, Sakai H, Abe M (2005) Direct synthesis of mesoporous titania particles having a crystalline wall. J Am Chem Soc 127(47):16396–16397
10. Leghari SAK, Sajjad S, Zhang J (2013) Large mesoporous micro-spheres of WO_3/TiO_2 composite with enhanced visible light photo activity. RSC Adv 3(35):15354
11. Sheng Q, Yuan S, Zhang J, Chen F (2006) Synthesis of mesoporous titania with high photocatalytic activity by nanocrystalline particle assembly. Microporous Mesoporous Mater 87(3):177–184
12. Wang Y, Xu H, Wang X, Zhang X, Jia H, Zhang L, Qiu J (2006) A general approach to porous crystalline TiO_2, $SrTiO_3$, and $BaTiO_3$ spheres. J Phys Chem B 110(28):13835–13840
13. Yue Y, Gao Z (2000) Synthesis of mesoporous TiO_2 with a crystalline framework. Chem Commun 18(18):1755–1756
14. Zhao B, Chen F, Liu H, Zhang J (2011) Mesoporous TiO_2-B nanowires synthesized from tetrabutyl titanate. J Phys Chem Solids 72(3):201–206
15. Li Y, Lee N, Lee E, Song J, Kim SJ (2004) The characterization and photocatalytic properties of mesoporous rutile TiO_2 powder synthesized through self-assembly of nano crystals. Chem Phys Lett 389(1–3):124–128
16. Fukumoto S, Kitano M, Takeuchi M, Matsuoka M, Anpo M (2008) Photocatalytic hydrogen production from aqueous solutions of alcohol as model compounds of biomass using visible light-responsive TiO_2 thin films. Catal Lett 127(1–2):39–43
17. Kikuchi H, Kitano M, Takeuchi M, Matsuoka M, Anpo M, Kamat PV (2006) Extending the photoresponse of TiO_2 to the visible light region: photoelectrochemical behavior of TiO_2 thin films prepared by the radio frequency magnetron sputtering deposition method. J Phys Chem B 110(11):5537–5541
18. Kitano M, Takeuchi M, Matsuoka M, Thomas JM, Anpo M (2005) Preparation of visible light-responsive TiO_2 thin film photocatalysts by an RF magnetron sputtering deposition method and their photocatalytic reactivity. Chem Lett 34(4):616–617
19. Kitano M, Tsujimaru K, Anpo M (2006) Decomposition of water in the separate evolution of hydrogen and oxygen using visible light-responsive TiO_2 thin film photocatalysts: effect of the work function of the substrates on the yield of the reaction. Appl Catal A-Gen 314(2):179–183
20. Buchel G, Denoyel R, Llewellyn PL, Rouquerol J (2001) In situ surfactant removal from MCM-type mesostructures by ozone treatment. J Mater Chem 11(2):589–593
21. Hitz S, Prins R (1997) Influence of template extraction on structure, activity, and stability of MCM-41 catalysts. J Catal 168(2):194–206
22. Tian B, Liu X, Yu C, Gao F, Luo Q, Xie S, Tu B, Zhao D (2002) Microwave assisted template removal of siliceous porous materials. Chem Commun 11(11):1186–1187
23. Van Grieken R, Calleja G, Stucky GD, Melero JA, García RA, Iglesias J (2003) Supercritical fluid extraction of a nonionic surfactant template from SBA-15 materials and consequences on the porous structure. Langmuir 19(9):3966–3973
24. Yang C, Zibrowius B, Schmidt W, Schüth F (2004) Stepwise removal of the copolymer template from mesopores and micropores in SBA-15. Chem Mater 16(15):2918–2925

25. Yamashita H, Harada M, Misaka J, Takeuchi M, Ikeue K, Anpo M (2002) Degradation of propanol diluted in water under visible light irradiation using metal ion-implanted titanium dioxide photocatalysts. J Photoch Photobio A 148(1–3):257–261
26. Tian B, Zhang J, Tong T, Chen F (2008) Preparation of Au/TiO_2 catalysts from Au(I)-thiosulfate complex and study of their photocatalytic activity for the degradation of methyl orange. Appl Catal B-Environ 79(4):394–401
27. Yuan S, Sheng Q, Zhang J, Chen F, Anpo M, Zhang Q (2005) Synthesis of La^{3+} doped mesoporous titania with highly crystallized walls. Microporous Mesoporous Mater 79 (1–3):93–99
28. Yuan S, Sheng Q, Zhang J, Chen F, Anpo M, Dai W (2006) Synthesis of Pd nanoparticles in La-doped mesoporous titania with polycrystalline framework. Catal Lett 107(1–2):19–24
29. Yuan X, Zhang J, Anpo M, He D (2010) Synthesis of Fe^{3+} doped ordered mesoporous TiO_2 with enhanced visible light photocatalytic activity and highly crystallized anatase wall. Res Chem Intermed 36(1):83–93
30. Sajjad S, Leghari SAK, Zhang J (2013) Copper impregnated ionic liquid assisted mesoporous titania: visible light photocatalyst. RSC Adv 3(31):12678
31. He C, Tian B, Zhang J (2010) Thermally stable SiO_2-doped mesoporous anatase TiO_2 with large surface area and excellent photocatalytic activity. J Colloid Interface Sci 344(2):382–389
32. Wu Y, Xing M, Tian B, Zhang J, Chen F (2010) Preparation of nitrogen and fluorine co-doped mesoporous TiO_2 microsphere and photodegradation of acid orange 7 under visible light. Chem Eng J 162(2):710–717
33. He C, Tian B, Zhang J (2010) N, B, Si-tridoped mesoporous TiO_2 with high surface area and excellent visible-light photocatalytic activity. Res Chem Intermed 36(4):349–359
34. Hao H, Zhang J (2009) The study of Iron (III) and nitrogen co-doped mesoporous TiO_2 photocatalysts: synthesis, characterization and activity. Microporous Mesoporous Mater 121 (1–3):52–57
35. Ma Y, Xing M, Zhang J, Tian B, Chen F (2012) Synthesis of well ordered mesoporous Yb, N co-doped TiO_2 with superior visible photocatalytic activity. Microporous Mesoporous Mater 156:145–152
36. Qiu B, Xing M, Zhang J (2014) Mesoporous TiO_2 nanocrystals grown in situ on graphene aerogels for high photocatalysis and lithium-ion batteries. J Am Chem Soc 136(16):5852–5855
37. Dong C, Xing M, Zhang J (2016) Double-cocatalysts promote charge separation efficiency in CO_2 photoreduction: spatial location matters. Mater Horiz 3:608–612
38. Anderson C, Bard AJ (1995) An improved photocatalyst of TiO_2/SiO_2 prepared by a sol-gel synthesis. J Phys Chem 99(24):9882–9885
39. Gao X, Wachs IE (1999) Titania-silica as catalysts: molecular structural characteristics and physico-chemical properties. Catal Today 51(2):233–254
40. Dagan G, Sampath S, Lev O (1995) Preparation and utilization of organically modified silica-titania photocatalysts for decontamination of aquatic environments. Chem Mater 7(3):446–453
41. Klein S, Thorimbert S, Maier WF (1996) Amorphous microporous titania-silica mixed oxides: preparation, characterization, and catalytic redox properties. J Catal 163(2):476–488
42. Pabón E, Retuert J, Quijada R, Zarate A (2004) TiO_2-SiO_2 mixed oxides prepared by a combined sol-gel and polymer inclusion method. Microporous Mesoporous Mater 67 (2–3):195–203
43. Li Z, Hou B, Xu Y, Wu D, Sun Y (2005) Hydrothermal synthesis, characterization, and photocatalytic performance of silica-modified titanium dioxide nanoparticles. J Colloid Interface Sci 288(1):149–154
44. Xing M, Qi D, Zhang J, Chen F, Tian B, Bagwas S, Anpo M (2012) Super-hydrophobic fluorination mesoporous MCF/TiO_2 composite as a high-performance photocatalyst. J Catal 294:37–46
45. Gun'ko VM, Zarko VI, Turov VV, Leboda R, Chibowski E, Holysz L, Pakhlov EM, Voronin EF, Dudnik VV, Gornikov YI (1998) CVD-Titania on Fumed silica substrate. J Colloid Interface Sci 198(1):141–156

46. Fan G, Zou B, Cheng S, Zheng L (2010) Ligandless palladium supported on SiO_2-TiO_2 as effective catalyst for Suzuki reaction. J Ind Eng Chem 16(2):220–223
47. Mei F, Liu C, Zhang L, Ren F, Zhou L, Zhao W, Fang Y (2006) Microstructural study of binary TiO_2:SiO_2 nanocrystalline thin films. J Cryst Growth 292(1):87–91
48. Siddiquey IA, Furusawa T, Sato M, Honda K, Suzuki N (2008) Control of the photocatalytic activity of TiO_2 nanoparticles by silica coating with polydiethoxysiloxane. Dyes Pigments 76 (3):754–759
49. Li D (2004) Study on the fluorescence properties of benzopyrylium salt in Ti-HMS. Dyes Pigments 63(1):71–76
50. Zhao W, Li D, He B, Zhang J, Huang J, Zhang L (2005) The photoluminescence of coumarin derivative encapsulated in MCM-41 and Ti-MCM-41. Dyes Pigments 64(3):265–270
51. He C, Tian B, Zhang J (2009) Synthesis of thermally stable and highly ordered bicontinuous cubic mesoporous titania-silica binary oxides with crystalline framework. Microporous Mesoporous Mater 126(1–2):50–57
52. Chen C, Ma W, Zhao J (2010) Semiconductor-mediated photodegradation of pollutants under visible-light irradiation. Chem Soc Rev 39(11):4206–4219
53. Aguado J, van Grieken R, López-Muñoz MJ, Marugán J (2002) Removal of cyanides in wastewater by supported TiO_2-based photocatalysts. Catal Today 75(1–4):95–102
54. Fujishima A, Honda K (1972) Electrochemical photolysis of water at a semiconductor electrode. Nature 238(5358):37–38
55. Horiuchi Y, Toyao T, Takeuchi M, Matsuoka M, Anpo M (2013) Recent advances in visible-light-responsive photocatalysts for hydrogen production and solar energy conversion-from semiconducting TiO_2 to MOF/PCP photocatalysts. Phys Chem Chem Phys 15 (32):13243–13253
56. Niphadkar PS, Chitale SK, Sonar SK, Deshpande SS, Joshi PN, Awate SV (2014) Synthesis, characterization and photocatalytic behavior of TiO_2-SiO_2 mesoporous composites in hydrogen generation from water splitting. J Mater Sci 49(18):6383–6391
57. Xing M, Zhang J, Qiu B, Tian B, Anpo M, Che M (2014) A brown mesoporous TiO_{2-x}/MCF composite with an extremely high quantum yield of solar energy photocatalysis for H_2 evolution. Small 11(16):1920–1929
58. Hill RJ, Long DL, Champness NR, Hubberstey P, Schröder M (2005) New approaches to the analysis of high connectivity materials: design frameworks based upon 44- and 63-subnet tectons. Acc Chem Res 38(4):335–348
59. Yaghi OM, O'keeffe M, Ockwig NW, Chae HK, Eddaoudi M, Kim J (2003) Reticular synthesis and the design of new materials. Nature 423(6941):705–714
60. Kitagawa S, Kitaura R, Si N (2004) Functional porous coordination polymers. Angew Chem Int Ed 43(18):2334–2375
61. Moulton B, Zaworotko MJ (2001) From molecules to crystal engineering: supramolecular isomerism and polymorphism in network solids. Chem Rev 101(6):1629–1658
62. Seo JS, Whang D, Lee H, Im Jun S, Oh J, Jeon YJ, Kim K (2000) A homochiral metal-organic porous material for enantioselective separation and catalysis. Nature 404(6781):982–986
63. Zhou T, Du Y, Borgna A, Hong J, Wang Y, Han J, Zhang W, Xu R (2013) Post-synthesis modification of a metal-organic framework to construct a bifunctional photocatalyst for hydrogen production. Energy Environ Sci 6(11):3229–3234
64. Horiuchi Y, Toyao T, Saito M, Mochizuki K, Iwata M, Higashimura H, Anpo M, Matsuoka M (2012) Visible-light-promoted photocatalytic hydrogen production by using an amino-functionalized Ti (IV) metal-organic framework. J Phys Chem C 116(39):20848–20853
65. Wang C, DeKrafft KE, Lin W (2012) Pt nanoparticles@photoactive metal-organic frameworks: efficient hydrogen evolution via synergistic photoexcitation and electron injection. J Am Chem Soc 134(17):7211–7214
66. Fateeva A, Chater PA, Ireland CP, Tahir AA, Khimyak YZ, Wiper PV, Darwent JR, Rosseinsky MJ (2012) A water-stable porphyrin-based metal-organic framework active for visible-light photocatalysis. Angew Chem 124(30):7558–7562

67. Kataoka Y, Sato K, Miyazaki Y, Masuda K, Tanaka H, Naito S, Mori W (2009) Photocatalytic hydrogen production from water using porous material $[Ru_2(p\text{-}BDC)_2]_n$. Energy Environ Sci 2 (4):397–400
68. Xiao J, Shang Q, Xiong Y, Zhang Q, Luo Y, Yu S, Jiang H (2016) Boosting photocatalytic hydrogen production of a metal-organic framework decorated with platinum nanoparticles: the platinum location matters. Angew Chem 128(32):9535–9539
69. Gomes Silva C, Luz I, Llabrés i, Xamena FX, Corma A, García H (2010) Water stable Zr-benzenedicarboxylate metal-organic frameworks as photocatalysts for hydrogen generation. Chem-Eur J 16(36):11133–11138
70. Fu Y, Sun D, Chen Y, Huang R, Ding Z, Fu X, Li Z (2012) An amine-functionalized titanium metal-organic framework photocatalyst with visible-light-induced activity for CO_2 reduction. Angew Chem 124(14):3420–3423
71. Alvaro M, Carbonell E, Ferrer B, Llabrés i, Xamena FX, Garcia H (2007) Semiconductor behavior of a metal-organic framework (MOF). Chem-Eur J 13(18):5106–5112
72. Tachikawa T, Choi JR, Fujitsuka M, Majima T (2008) Photoinduced charge-transfer processes on MOF-5 nanoparticles: elucidating differences between metal-organic frameworks and semiconductor metal oxides. J Phys Chem C 112(36):14090–14101
73. Yang H, He X, Wang F, Kang Y, Zhang J (2012) Doping copper into ZIF-67 for enhancing gas uptake capacity and visible-light-driven photocatalytic degradation of organic dye. J Mater Chem 22(41):21849–21851
74. Anpo M, Yamashita H, Ikeue K, Fujii Y, Zhang S, Ichihashi Y, Park DR, Suzuki Y, Koyano K, Tatsumi T (1998) Photocatalytic reduction of CO_2 with H_2O on Ti-MCM-41 and Ti-MCM-48 mesoporous zeolite catalysts. Catal Today 44(1–4):327–332
75. Takeuchi M, Dohshi S, Eura T, Anpo M (2003) Preparation of titanium-silicon binary oxide thin film photocatalysts by an ionized cluster beam deposition method. Their photocatalytic activity and photoinduced super-hydrophilicity. J Phys Chem B 107(51):14278–14282
76. Takeuchi M, Yamashita H, Matsuoka M, Anpo M, Hirao T, Itoh N, Iwamoto N (2000) Photocatalytic decomposition of NO on titanium oxide thin film photocatalysts prepared by an ionized cluster beam technique. Catal Lett 66(3):185–187
77. Anpo M, Aikawa N, Kubokawa Y, Che M, Louis C, Giamello E (1985) Photoluminescence and photocatalytic activity of highly dispersed titanium oxide anchored onto porous Vycor glass. J Phys Chem 89(23):5017–5021
78. Anpo M, Yamashita H, Ichihashi Y, Fujii Y, Honda M (1997) Photocatalytic reduction of CO_2 with H_2O on titanium oxides anchored within micropores of zeolites: effects of the structure of the active sites and the addition of Pt. J Phys Chem B 101(14):2632–2636
79. Anpo M (1997) In situ characterization of highly dispersed catalysts included within zeolite cavities and their photocatalytic reactivities. Nouv Cim D 19(11):1641–1648
80. Yamashita H, Anpo M (2004) Application of an ion beam technique for the design of visible light-sensitive, highly efficient and highly selective photocatalysts: ion-implantation and ionized cluster beam methods. Catal Surv Jpn 8(1):35–45
81. Hu Y, Rakhmawaty D, Matsuoka M, Takeuchi M, Anpo M (2006) Synthesis, characterization and photocatalytic reactivity of Ti-containing micro- and mesoporous materials. J Porous Mater 13(3–4):335–340
82. Anpo M, Chiba K (1992) Photocatalytic reduction of CO_2 on anchored titanium oxide catalysts. J Mol Catal 74(1–3):207–212
83. Yamashita H, Shiga A, Kawasaki S-i, Ichihashi Y, Ehara S, Anpo M (1995) Photocatalytic synthesis of CH_4 and CH_3OH from CO_2 and H_2O on highly dispersed active titanium oxide catalysts. Energy Convers Manag 36(6–9):617–620
84. Ikeue K, Yamashita H, Anpo M (1999) Photocatalytic reduction of CO_2 with H_2O on titanium oxides prepared within the FSM-16 mesoporous zeolite. Chem Lett 28(11):1135–1136
85. Ikeue K, Yamashita H, Anpo M, Takewaki T (2001) Photocatalytic reduction of CO_2 with H_2O on Ti-β zeolite photocatalysts: effect of the hydrophobic and hydrophilic properties. J Phys Chem B 105(35):8350–8355

86. Ikeue K, Nozaki S, Ogawa M, Anpo M (2002) Characterization of self-standing Ti-containing porous silica thin films and their reactivity for the photocatalytic reduction of CO_2 with H_2O. Catal Today 74(3–4):241–248
87. Yamashita H, Honda M, Harada M, Ichihashi Y, Anpo M, Hirao T, Itoh N, Iwamoto N (1998) Preparation of titanium oxide photocatalysts anchored on porous silica glass by a metal ion-implantation method and their photocatalytic reactivities for the degradation of 2-propanol diluted in water. J Phys Chem B 102(52):10707–10711
88. Ikeue K, Nozaki S, Ogawa M, Anpo M (2002) Photocatalytic reduction of CO_2 with H_2O on Ti-containing porous silica thin film photocatalysts. Catal Lett 80(3–4):111–114
89. Shioya Y, Ikeue K, Ogawa M, Anpo M (2003) Synthesis of transparent Ti-containing mesoporous silica thin film materials and their unique photocatalytic activity for the reduction of CO_2 with H_2O. Appl Catal A-Gen 254(2):251–259
90. Anpo M, Thomas JM (2006) Single-site photocatalytic solids for the decomposition of undesirable molecules. Chem Commun 31(0):3273–3278